Journal of Solid State Chemistry 183 (2010) 784–788

Contents lists available at ScienceDirect

Journal of Solid State Chemistry

journal homepage: www.elsevier.com/locate/jssc

Zr_2Ir_6B with an eightfold superstructure of the cubic perovskite-like boride $ZrIr_3B_{0.5}$: Synthesis, crystal structure and bonding analysis

Martin Hermus, Boniface P.T. Fokwa *

Institute of Inorganic Chemistry, RWTH Aachen University, Landoltweg 1, 52056 Aachen, Germany

ARTICLE INFO

Article history:
Received 26 November 2009
Received in revised form
15 January 2010
Accepted 24 January 2010
Available online 1 February 2010

Keywords:
Zirconium iridium boride
Double cubic perovskite
Structure
COHP
Cluster

ABSTRACT

Single phase powder samples and single crystals of Zr_2Ir_6B were successfully synthesized by arc-melting the elements in a water-cooled copper crucible under an argon atmosphere. Superstructure reflections were observed both on powder and on single crystal diffraction data, leading to an eightfold superstructure of $ZrIr_3B_x$ phase. The new phase, which has a metallic luster, crystallizes in space group $Fm\bar{3}m$ (no. 225) with the lattice parameters $a=7.9903(4)$ Å, $V=510.14(4)$ Å^3. Its crystal structure was refined on the basis of powder as well as single crystal data. The single crystal refinement converged to $R_1=0.0239$ and $wR_2=0.0624$ for all 88 unique reflections and 6 parameters. Zr_2Ir_6B is isotypic to Ti_2Rh_6B and its structure can be described as a defect double perovskite, $A_2BB'O_6$, where the A site is occupied by zirconium, the B site by boron, the O site by iridium but the B' site is vacant, leading to the formation of empty and boron-filled octahedral Ir_6 clusters. According to the result of tight-binding electronic structure calculations, Ir–B and Ir–Zr interactions are mainly responsible for the structural stability of the phase. According to COHP bonding analysis, the strongest bonding occurs for the Ir–B contacts, and the Ir–Ir bonding within the empty clusters is two times stronger than that in the BIr_6 octahedra.

1. Introduction

Among the large family of perovskites, a group of cubic intermetallic perovskites with the general formula AM_3X [1], where A and M are metals and X is B, C, or N have drawn a great deal of attention lately due to their interesting physical properties [2–5]. YRh_3B possesses the hardness value of 8 GPa [6], whereas YRh_3B [7] and $MgNi_3C$ [8] are superconductors with transition temperatures of 0.8 and 8 K, respectively. They all crystallize with the simple cubic perovskite structure in space group $Pm\bar{3}m$ (no. 221).

The majority of the boron-containing phases usually show a boron non-stoichiometry and are often reported as AM_3B_x ($0<x\leq 1$) [1,6,9,10]. Up to now, superstructure reflections have not been reported in the X-ray powder or single crystal diffraction data of these phases. As a consequence boron ordering is rare. In fact the observation of these superstructure reflections may lead to a change in the chemical formula depending on the obtained space group as already demonstrated in the perovskite family of oxides [11]. Ti_2Rh_6B (vacant double perovskite-like, space group $Fm\bar{3}m$, no. 225) [12] is the first phase where a boron ordering was observed due to the presence of the 1/2 1/2 1/2-type superstructure reflections in both X-ray single crystal and powder diffraction data. However, electron diffraction patterns have also revealed the presence of the same type of superstructure reflections together with some satellite ones in $CeRh_3B_x$ ($0.4\leq x\leq 0.5$) [13] and $ScRh_3B_x$ ($0.5\leq x\leq 0.75$) [14] phases. These findings indicate that the structures of these non-stoichiometric perovskite borides are actually only the average structures. Even in $CePd_3B_{0.13}$ the eithfold superstructure ($Ce_8Pd_{24}Sb$-type[15]) found in related $Ce_8Pd_{24}M$ ($8xCePd_3M_{0.13}$) phases (M=Al, Ga, In, Ge, Sn, Pb), was not observed [16]. $ZrIr_3B_x$ ($0<x\leq 0.5$) synthesized in the late 1970s make no exception as it was structurally described also as a simple cubic perovskite [10]. We have been able to synthesize high quality powder samples and single crystals for the composition with $x=0.5$ and its X-ray single crystal and powder diffraction data show the 1/2 1/2 1/2-type superstructure reflections. Herein we report on the synthesis, crystal and electronic structure of Zr_2Ir_6B.

2. Experimental

2.1. Synthesis

Polycrystalline samples and single crystals of Zr_2Ir_6B were synthesized by arc-melting the elements in a water-cooled copper crucible under an argon atmosphere using a tungsten tip as a second electrode. The starting materials, zirconium (powder, 99.9%, Alfa Aesar), iridium (powder, 99.95%, Alfa Aesar) and boron

* Corresponding author.
E-mail address: boniface.fokwa@ac.rwth-aachen.de (B.P.T. Fokwa).

0022-4596/$ - see front matter © 2010 Elsevier Inc. All rights reserved.
doi:10.1016/j.jssc.2010.01.026

(amorphous powder, 99%, Fluka), were weighed in the respective atomic ratios, pressed into pellets and arc-melted under argon until homogeneous melting; the argon was purified prior to use over silica gel, molecular sieves, and titanium sponge (950 K). The reaction products were remelted several times to ensure good homogeneity of the samples. Weight losses during the melting process were negligible. A silver-like product with metallic luster was obtained with several single crystals suitable for X-ray structure analysis. The sample is stable in air as a compact bulk as well as finely ground powder.

The purity of the sample was checked by X-ray powder diffraction through Guinier powder diffractograms using CuKα_1 radiation (λ=1.54059 Å) and silicon as an internal standard. The lattice parameters were refined on the basis of powder data with the program WinXPOW [17]. The Zr:Ir ratio was checked by energy-dispersive X-ray analysis (EDX) on a high-resolution low-energy SEM of the type LEO 1530 (Oberkochen, Germany) equipped with an EDX system of the type INCA (Oxford, England).

2.2. Crystal structure determination

2.2.1. Rietveld refinement

A high quality powder diffractogram was measured (2θ range: 15–120°, with 0.01° and 220 second per step) on a STOE STADI P diffractometer equipped with a position sensitive detector (PSD), using Germanium (1 1 1) monochromatized Cu$K\alpha_1$ radiation (λ=1.54059 Å). The crystal structure was refined using the Ti_2Rh_6B structural model by full-matrix least-squares refinement implemented in the FULLPROF program [18].

2.2.2. Single crystal refinement

A single crystal of suitable size was fixed on top of a glass capillary and X-ray data were collected on a CCD single-crystal diffractometer (Bruker SMART APEX) with graphite-monochromatized Mo$K\alpha$ radiation (λ=0.71073 Å). The X-ray intensities were corrected with respect to absorption using a semi-empirical procedure [19]. The crystal structure was solved by direct methods and refined by full-matrix least-squares refinement (based on F^2 [20]) using anisotropic displacement parameters for all atoms. All relevant crystallographic data and experimental details of the data collection are listed in Table 1. A listing of all refinement data and data collection is available.[1]

2.3. Electronic structure calculations

The all-electron, scalar-relativistic electronic structure calculations were performed using the linear muffin-tin orbital (LMTO) method [21–24]. The electronic energy was calculated via density-functional theory using the von Barth and Hedin parameterization of the local exchange-correlation potential [25]. Diagonalization and integration in reciprocal space were performed with the help of an improved tetrahedron method [26]. All calculations were checked for convergence of energies, orbital moments, and calculated crystal orbital Hamilton populations (COHP, [27]) with respect to the number of k points. The basis set was composed of short-ranged [28] atom-centered TB-LMTOs as provided by the TB-LMTO 4.7 program [29]. The atomic spheres were sized, based on atomic Hartree potentials, at 1.948, 1.344 and 1.032 Å for Zr, Ir and B, respectively.

[1] More details on the structure determination may be obtained from the Fachinformationszentrum Karlsruhe (e-mail address: crysdata@fiz-karlsruhe.de), D-76344 Eggenstein-Leopoldshafen, Germany, on quoting the CSD depository number CSD 421246.

Table 1
Crystallographic and structure refinement data of Zr_2Ir_6B.

Formula	Zr_2Ir_6B
Formula weight; F(0 0 0)	1346.45 g mol^{-1}; 2188
Crystal size; color	0.08 × 0.04 × 0.03 mm^3; silver
Space group; Z	$Fm\bar{3}m$ (no. 225); 4
Lattice parameters	a=7.9906(16) Å V=510.20(18) Å^3
Lattice parameters (powder data)	a=7.9903(4) Å V=510.14(4) Å^3
Calc. density	17.529 g cm^{-3}
Abs. correction	Semi-empirical
Abs. Coefficient	159.58 mm^{-1}
T_{min}; T_{max}	0.020; 0.087
Diffractometer	Bruker APEX CCD, Mo$K\alpha$, graphite monochromator
θ-range	5.10° ≤ θ ≤ 35.68°
hkl-range	−13 ≤ h ≤ 9 −11 ≤ k ≤ 13 −10 ≤ l ≤ 12
No. of reflections; R_{int}	1377; 0.0130
No. of independent reflections	88
No. of parameters	6
Refinement	SHELX-97 [9], full matrix against F^2
R_1; wR_2 (all I)	0.0239; 0.0624
GooF	1.369
Diff. peak/hole	2.454/−2.965 e Å^{-3}

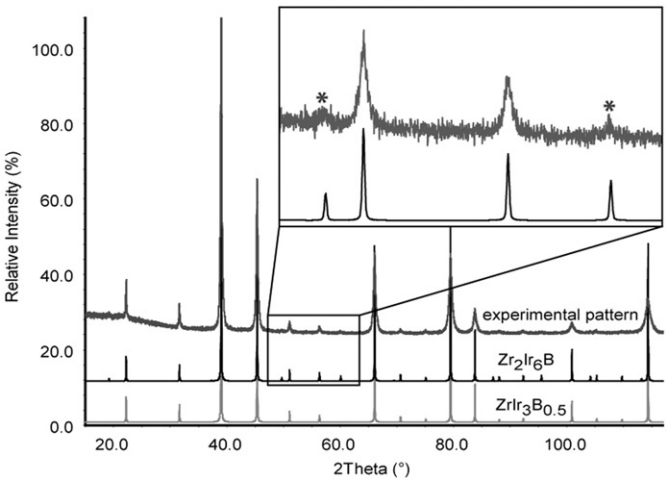

Fig. 1. Comparisons of calculated ($ZrIr_3B_{0.5}$ and Zr_2Ir_6B structural models) with measured (Zr_2Ir_6B) X-ray powder patterns. An enlarged part of the diffractograms shows some superstructure reflections (see asterisks).

3. Results and discussion

3.1. Crystal chemistry

The observed powder X-ray diffraction pattern of Zr_2Ir_6B showed, in addition to reflections of the $ZrIr_3B_{0.5}$ phase, also weak reflections that could be indexed (see Fig. 1) and the refinement leads to a doubling of the lattice parameter of $ZrIr_3B_{0.5}$ phase, a=7.9903(4) Å. Because the same superstructure reflections were observed in the Ti_2Rh_6B phase [12], its crystal structure was used as model for the Rietveld refinement. After substituting Ti with Zr and Rh with Ir the refinement converged easily (see Fig. 2) with R-values lower than 3%. Energy-dispersive X-ray analysis on several selected crystals confirmed the metal ratio used, as expected from this single phase synthesis. In addition, these

results were confirmed and further extended by single crystal structure refinement. The lattice parameters obtained from the single crystal data were nearly the same as those obtained from powder analysis (see Table 1). The structure could be solved from the single crystal data by direct methods. The subsequent refinement yielded the residual *R*-values given in Table 1. All atoms could be refined anisotropically (see Table 2). The doubling of the lattice parameter *a* implies an eightfold superstructure of the $ZrIr_3B_{0.5}$ simple cubic structure leading to 4 formula units in the unit cell of Zr_2Ir_6B (see Fig. 3).

Since $ZrIr_3B_x$ has a homogeneity range ($0 < x \leq 0.5$), it is well possible that Zr_2Ir_6B also shows a small homogeneity range. We have therefore tried to refine the boron occupancy (both on the single crystal and the powder data), but no significant deviation from the title formula was observed. The atomic positions are listed together with displacement parameters in Table 2. Table 3 provides a listing of selected bond lengths and respective ICOHP values.

As mentioned above, Zr_2Ir_6B is isostructural with Ti_2Rh_6B, the only difference being the replacement in the later of the 3*d* (Ti) and 4*d* (Rh) transition metals by the corresponding next higher analogues in the same group of the periodic table. This element substitution induces an increase of the unit cell volume of Zr_2Ir_6B by roughly 32 Å^3, if compared to that of Ti_2Rh_6B. Two different types of substitutions may also be imagined using these elements, namely a combination of 3*d* with 5*d* or 4*d* with 4*d* transition metals, leading, respectively, to the hypothetical "Ti_2Ir_6B" and "Zr_2Rh_6B" phases, whose volumes should lie between those of Ti_2Rh_6B and Zr_2Ir_6B. The authors who discovered $ZrIr_3B_x$ ($0 < x \leq 0.5$) also synthesize $ZrRh_3B_x$ ($0 < x \leq 1$) [10] but the corresponding "$TiIr_3B_x$" phase is still unknown. It is well possible that the same superstructure reflections observed in this work can also be found in a high quality diffraction pattern of $ZrRh_3B_{0.5}$, which will then induce its formulation as "Zr_2Rh_6B". In fact, as mentioned in the introduction, the structure of all intermetallic boride phases crystallizing with the simple cubic perovskite structure should be revised. However, the synthesis of high quality powder or single crystal data is the prerequisite for the observation of superstructure reflections.

In the crystal structure of Zr_2Ir_6B, zirconium occupies the Wyckoff position 8*c* (see Table 2) and is surrounded by 12 iridium atoms to form a cuboctahedron. Iridium occupies the position 24*e* and is surrounded by four zirconium atoms and eight other iridium atoms to also form a cuboctahedron but here one quadratic face of the cuboctahedron is centered by a boron atom. Boron lies at the position 4*e* and is octahedrally surrounded by six iridium atoms.

The crystal structure of Zr_2Ir_6B can be described as a double perovskite $A_2BB'O_6$ where the *A* site is occupied by zirconium, the *B* site by boron, the *O* site by iridium but the *B*′ site is vacant. As shown in Fig. 4a, isolated BIr_6 octahedra adopt the motif of a face-centered cubic structure. The resulting octahedral sites are vacant, leading to the formation of empty Ir_6 clusters (highlighted in Fig. 4b), and both entities are linked with each other via their corner iridium atoms.

3.2. Electronic structure and chemical bonding

The chemical bonding in Zr_2Ir_6B was investigated by LMTO band structure calculations. The DOS in the valence region exhibits significant iridium character with zirconium and boron levels contributing slightly from −9 eV up to the Fermi level (Fig. 5a). Because of the non-vanishing DOS at the Fermi level, the phase is predicted to be a metal, as expected for this intermetallic compound. The Fermi level lies ca. 1 eV below a deep pseudogap

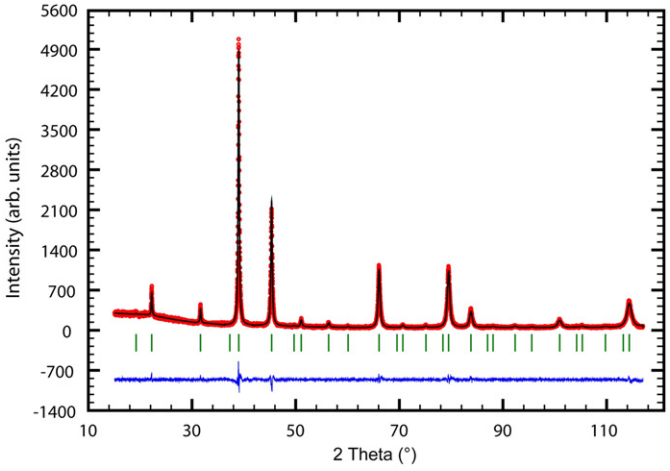

Fig. 2. Rietveld refinement of the X-ray powder pattern of the Zr_2Ir_6B-product showing measured and fitted intensities (top), the position of the Bragg peaks (middle), and the difference intensity curve (bottom).

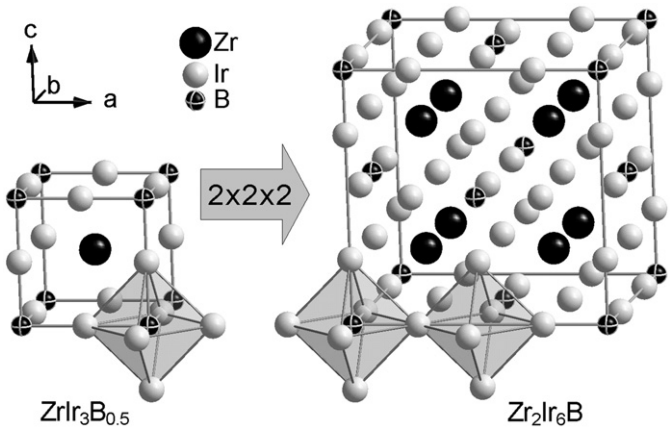

Fig. 3. Comparison of the crystal structure of $ZrIr_3B_{0.5}$ (left) with its eightfold superstructure Zr_2Ir_6B (right). In $ZrIr_3B_{0.5}$ (left) only the BIr_6 octahedra are present whereas in Zr_2Ir_6B (right) there are additional empty Ir_6 octahedral clusters.

Table 2
Atomic coordinates and displacement parameters (Å^2) of Zr_2Ir_6B.

Atom	Wyckoff position	*x*	*y*	*z*	U_{eq}	U_{11}	$U_{33}=U_{22}$
Zr	8*c*	1/4	1/4	1/4	0.0045(5)	0.0044(4)	U_{11}
Ir	24*e*	0.25526(5)	0	0	0.0032(2)	0.0041(3)	0.0027(2)
B	4*b*	0	0	0	0.026(9)	0.026(9)	U_{11}

U_{eq} is defined as 1/3 of the trace of the orthogonalized U_{ij} tensors, $U_{13}=U_{23}=U_{12}=0$.

Table 3
Selected bond lengths (d (Å)) and ICOHP (eV/bond) values of Zr_2Ir_6B and $ZrIr_3$.

	d (Å)	ICOHP (eV/bond)	Related example	d (Å)	ICOHP (eV/bond)
B–Ir	2.0396(6)	−2.06	–		
Zr–Ir	2.8254(6)	−0.99	$ZrIr_3$	2.788	−0.68
Ir–Ir (Ir_6)	2.7654(8)	−0.74	$ZrIr_3$	2.788	−0.86
Ir–Ir (Ir_6B)	2.8845(8)	−0.37			

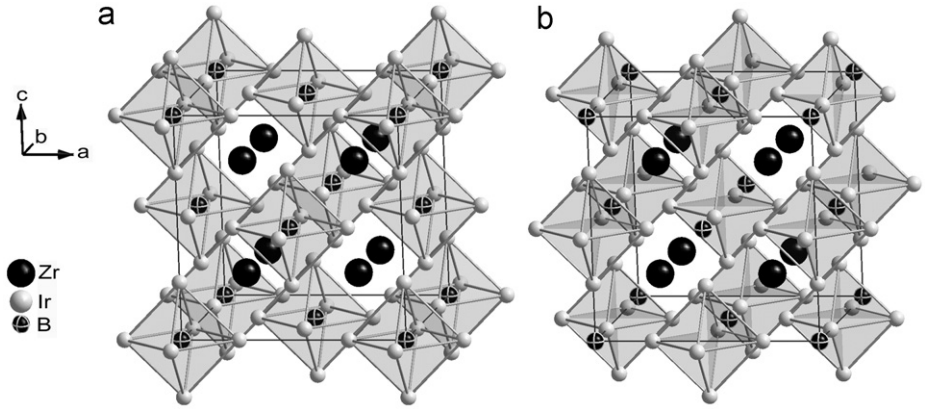

Fig. 4. Perspective views of the crystal structure of Zr_2Ir_6B highlighting (a) the BIr_6 octahedra and (b) the empty octahedral Ir_6 cluster.

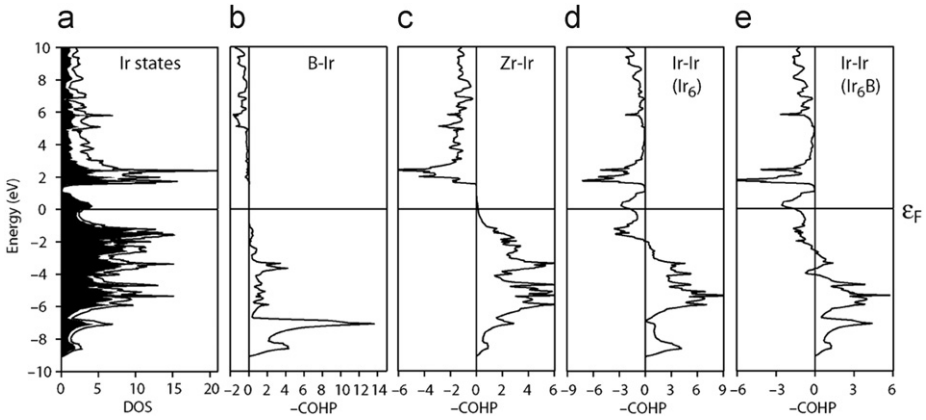

Fig. 5. (a) Total and partial DOS for Zr_2Ir_6B, COHP curves for (b) the six B–Ir bonds, (c) the twelve Zr–Ir bonds, (d) the twelve Ir–Ir bonds in the empty octahedral Ir_6 cluster and (e) the twelve Ir–Ir bonds in the BIr_6 octahedron.

in the DOS curve. Above the pseudogap, Zr valence orbitals show a greater contribution to the DOS.

A quantitative bonding analysis is possible on the basis of the shape and energy integrals (ICOHP) of the crystal orbital Hamilton populations (COHP). These results are summarized in Fig. 5b–e and Table 3, with ICOHP values for similar interatomic interactions in the related binary phase $ZiIr_3$ included for comparison. The COHP curves in Fig. 5 indicate that B–Ir and Zr–Ir orbital interactions are optimized in Zr_2Ir_6B: bonding orbitals are filled; antibonding orbitals are empty. The two types of Ir–Ir contacts show antibonding character around the Fermi level. This COHP analysis suggests that it is the heteroatomic B–Ir and Zr–Ir bonds that create the structural stability of Zr_2Ir_6B. In agreement with this assessment, the largest ICOHP values are found for the B–Ir and Zr–Ir contacts. The B–Ir distance, 2.04 Å, is even slightly shorter than the sum of their covalent radii (2.09 Å), in line with the strongest bonding interaction found for the B–Ir bond (ICOHP= −2.06 eV, see Fig. 5b). An even shorter distance is found in the simple cubic perovskite $ScIr_3B$ (2.00 Å) [30]. The ICOHP value (−0.99 eV, see Fig. 5c) for Zr–Ir bond also indicates significant orbital interactions, which occur in the binary intermetallic $ZrIr_3$ [31] as well (see Table 3), and is reflected in the average distance (2.82 Å) being shorter than the sum of metallic radii for CN 12 (2.96 Å [32]). Concerning the Ir–Ir interactions there exist two different types. First, one finds 12 short Ir–Ir contacts of ca. 2.76 Å in the empty Ir_6 cluster and, second, there are other 12 but wider Ir–Ir contacts of 2.88 Å in the filled BIr_6 octahedra. The analysis (Fig. 5d and e) evidences a net bonding effect for both but the energy integral for the Ir–Ir contact in the empty Ir_6 cluster (ICOHP= −0.74 eV/ bond) is twice as large as that of the same contact in the filled BIr_6 octahedra (ICOHP= −0.37 eV/ bond). The Ir–Ir bonding in the BIr_6 octahedron is

significantly weakened because too much electron density on iridium has gone into the heteroatomic B–Ir and Zr–Ir bonds. We also note that the 2.76 Å short (and strongly bonding) Ir–Ir contact (in Ir_6) is just slightly larger than the metallic iridium distance for CN 12 (2.71 Å, [32]) but shorter than the observed value (2.79 Å) in the empty Ir_6 cluster present in $ZrIr_3$ [31]. The much weaker 2.88 Å long Ir–Ir bond in the BIr_6 octahedra may be compared with even wider Ir–Ir distances such as those present in BIr_6 trigonal prisms of $Sc_3Ir_5B_2$ (2.95 Å, average) [33]. No Zr–Zr bonding interactions were found. In $ZrIr_3$, the ICOHP value of the Ir–Ir interaction is much larger than that of Zr–Ir (see Table 3). The reverse situation is observed in Zr_2Ir_6B, because much electron densities on the iridium atom have been engaged in the B–Ir bond, thereby weakening the Ir–Ir interactions.

The shapes of the DOS and COHP curves of this compound are similar to those of the isotypic Ti_2Rh_6B phase. However, the main difference between the two phases lies in the presence of a pseudogap in the DOS curve of Zr_2Ir_6B, which is absent in Ti_2Rh_6B.

4. Conclusions

We have successfully synthesized high quality powder samples and single crystals of Zr_2Ir_6B by arc-melting stoichiometric amounts of the elements. Zr_2Ir_6B is, besides Ti_2Rh_6B, only the second reported ordered intermetallic boride perovskite, and its structure is described as a vacancy-containing double perovskite characterized by empty Ir_6 clusters and filled BIr_6 octahedra. COHP analyses indicate that Ir–B and Zr–Ir interactions are responsible for the structural stability of the phase. In addition, there are likewise stronger Ir–Ir bonding interactions in the Ir_6 clusters than those present in the BIr_6 octahedra. The DOS predicts a metallic behavior for the compound with main contributions from the iridium 5*d* states, and a pseudogap is observed at ca. 1 eV above the Fermi level.

Acknowledgments

The authors thank Deutsche Forschungsgemeinschaft for financial support, Resi Zaunbrecher for the EDX analysis, and Dr. Paul Müller and Klaus Kruse for their technical support during the X-ray experiments.

Appendix A. Supplementary material

Supplementary data associated with this article can be found in the online version at doi:10.1016/j.jssc.2010.01.026.

References

[1] P. Villars, K. Cenzual, Pearson's Crystal Structure Database for Inorganic Compounds (on CD-ROM), Version 1.0, Materials Park, OH, USA, 2007/8.
[2] P. Rogl, L. Delong, J. Less-Common Met. 91 (1983) 97.
[3] H. Takei, T. Shishido, J. Less-Common Met. 97 (1984) 223.
[4] R.E. Schaak, M. Avdeev, W.-L. Lee, G. Lawes, H.W. Zandbergen, J.D. Jorgensen, N.P. Ong, A.P. Ramirez, R.J. Cava, J. Solid State Chem. 177 (2004) 1244.
[5] D. Music, J.M. Schneider, Appl. Phys. Lett. 88 (2006) 031914.
[6] T. Shishido, J. Ye, K. Kudou, S. Okada, K. Obara, T. Sugawara, M. Oku, K. Wagatsuma, H. Horiuchi, T. Fukuda, J. Alloys Compd. 291 (1999) 52.
[7] H. Takei, N. Kobayashi, H. Yamauchi, T. Shishido, T. Fukase, J. Less-Common Met. 125 (1986) 233.
[8] T. He, Q. Huang, A.P. Ramirez, Y. Wang, K.A. Regan, N. Rogado, M.A. Hayward, M.K. Haas, J.S. Slusky, K. Inumara, H.W. Zandbergen, N.P. Ong, R.J. Cava, Nature 411 (2001) 54.
[9] M. Oku, T. Shishido, T. Shinohara, Q. Sun, Y. Kawazoe, K. Nakajima, K. Wagatsuma, J. Solid State Chem. 177 (2004) 457.
[10] P. Rogl, H. Nowotny, J. Less-Common Met. 67 (1979) 41.
[11] J.C. Howard, B.J. Kennedy, P.M. Woodward, Acta Crystallogr. B 59 (2003) 463.
[12] B.P.T. Fokwa, B. Eck, R. Dronskowski, Z. Kristallogr. 221 (2006) 445.
[13] K. Yubuta, A. Nomura, T. Yamamura, T. Shishido, J. Alloys Compd. 451 (2008) 301.
[14] K. Yubuta, A. Nomura, K. Nakajima, T. Shishido, J. Alloys Compd. 471 (2009) 341.
[15] R.A. Gordon, F.J. DiSalvo, Z. Naturforsch. B 51 (1996) 52.
[16] C.D.W. Jones, R.A. Gordon, B.K. Cho, F.J. DiSalvo, J.S. Kim, G.R. Stewart, Physica B 262 (1999) 284.
[17] WinXPOW, V 1.06, STOE Cie., Darmstadt, 1999.
[18] J. Rodriguez-Carvajal, FULLPROF, Version 2.8, ILL, 2004.
[19] G.M. Sheldrick, SADABS, Universität Göttingen, 1996.
[20] G.M. Sheldrick, A short history of SHELX, Acta Crystallogr. A 64 (2008) 112.
[21] O.K. Andersen, Phys. Rev. B 12 (1975) 3060.
[22] H.L. Skriver, The LMTO Method, Springer-Verlag, Berlin, 1984.
[23] O.K. Andersen, Linear methods in band theory, in: P. Phariseau, W.H. Temmermann (Eds.), The Electronic Structure of Complex Systems, Proceedings of a NATO Advanced Study Institute, Plenum Press, 1984, pp. 11–66.
[24] O.K. Andersen, C. Arcangeli, R.W. Tank, T. Saha-Dasgupta, G. Krier, O. Jepsen, I. Dasgupta, Third-generation TB-LMTO, in: L. Colombo, A. Gonis, P. Turchi (Eds.), Tight-binding Approaches to Computational Materials Science, MRS Symposia Proceedings No. 91, Materials Research Society, Pittsburgh, 1998, pp. 3–34.
[25] U. von Barth, L. Hedin, J. Phys. C 5 (1972) 1629.
[26] P.E. Blöchl, O. Jepsen, O.K. Andersen, Phys. Rev. B 49 (1994) 16223.
[27] R. Dronskowski, P.E. Blöchl, J. Phys. Chem. 97 (1993) 8617.
[28] O.K. Andersen, O. Jepsen, Phys. Rev. Lett. 53 (1984) 2571.
[29] G. Krier, O. Jepsen, A. Burkhardt, O. K. Andersen, The TB-LMTO-ASA program, version 4.7, Max-Planck-Institut für Festkörperforschung Stuttgart.
[30] H. Holleck, J. Less-Common Met. 52 (1977) 167.
[31] A.E. Dwight, P.A. Beck, Trans. Metall. Soc. AIME 215 (1959) 976.
[32] L. Pauling, B. Kamb, Proc. Natl. Acad. Sci. USA 83 (1986) 3569.
[33] E.A. Nagelschmitz, W. Jung, Chem. Mater. 10 (1998) 3189.